Journal of Applied Polymer Science

Characterization of crystalline structure and free volume of polyamide 6/nitrile rubber elastomer thermoplastic vulcanizates: Effect of the processing additives

Ana Catarina de O. Gomes,[1] Bluma G. Soares,[2] Marcia G. Oliveira,[3] José C. Machado,[4†] Dario Windmöller,[4] Caio M. Paranhos [5]

[1]Department of Materials Engineering, Federal University of São Carlos, São Carlos, Brazil
[2]Institute of Macromolecules, Federal University of Rio de Janeiro, Rio de Janeiro, Brazil
[3]Division of Materials Processing and Characterization, National Institute of Technology, Rio de Janeiro, Brazil
[4]Positron Annihilation Spectroscopy Laboratory, Department of Chemistry, Federal University of Minas Gerais, Belo Horizonte, Brazil
[5]Polymer Laboratory, Department of Chemistry, Federal University of São Carlos, São Carlos São Paulo CEP 13565-905, Brazil
[†]In Memorian.
Correspondence to: C. M. Paranhos (E-mail: paranhos@ufscar.br)

ABSTRACT: Blends of polyamide 6 and nitrile rubber (PA6/NBR) dynamically vulcanized may generate innovative products for special purposes where both high temperature and chemical resistance are key factors. In this investigation, we show that the crystalline nature of the PA6 can be controlled in terms of its morphological aspects (degree of crystallinity, crystal size, and structure) as a consequence of the presence of NBR and processing additives. Our results indicate that this crystalline control is dependent on the plasticization caused by the processing additives. Furthermore, imide-like linkage formation was favored in the presence of ethylene-*co*-vinyl acetate (EVA)-*g*-maleic anhydride, resulting in changes in the molecular mobility of the PA6 matrix, crystallization parameters, and viscoelastic properties when compared to the others EVA additives. © 2017 Wiley Periodicals, Inc. J. Appl. Polym. Sci. **2017**, *134*, 45576.

KEYWORDS: blends; crosslinking; morphology; polyamides

Received 6 April 2017; accepted 23 July 2017
DOI: 10.1002/app.45576

INTRODUCTION

Elastomer thermoplastic vulcanizates (TPVs) are blends in which the elastomer component is dynamically vulcanized *in situ* during melt mixing with the thermoplastic component at high shear and elevated temperature. Therefore, TPVs can combine the processability of thermoplastics with the elastic properties of elastomers. They offer a substantial economic advantage with respect to fabrication of parts with great possibility of reuse and recycling. In order to achieve this unique characteristic, it is expected that the vulcanized elastomer particles have a diameter of a few micrometers and they must be dispersed in the thermoplastic matrix.[1–4]

In polymer blends with a semicrystalline matrix, the final properties are determined by several factors that influence the crystalline phase, such as state of dispersion of the rubber phase in the crystalline matrix; dimension and size distribution of the crystalline phase; internal structure of the crystallites; and adhesion between the rubber particles and the crystalline matrix. It is well established that the properties of various polymer blends are affected by the nature of the matrix crystalline structure and the extent of crystallinity.[5,6] For instance, Joseph *et al.*[7] investigated the melting and the crystallization behavior of isotatic polypropylene (PP)/nitrile rubber (NBR) blends. The presence of a small percentage of NBR reduced the average spherulite size of PP in the blend, and the blend ratio had a predominant effect on the crystalline parameters. Compatibilized blends of polyamide 6 (PA6) and ethylene-*co*-vinyl acetate copolymer grafted with maleic anhydride (EVA-*g*-MA) were studied by Bhattacharyya *et al.*[8] The overall crystallinity of the compatibilized blends decreased as compared to both uncompatibilized blends and pure PA6, suggesting that the reduced mobility of crystallizing chains was due to graft copolymer formation at the interface. In the case of TPVs, Liu *et al.*[9] studied the crystallization behavior of PA6/ethylene–propylene–diene rubber (EPDM) TPVs. The results showed that the EPDM did not act as a nucleating agent in the samples that were not dynamically vulcanized. In dynamically vulcanized samples, the EPDM rubber

did act as a nucleating agent and the addition of chlorinated polyethylene as compatibilizer improved the crystallization of PA6. Zhang *et al.*[10] showed that ultrafine fully vulcanized, carboxylic styrene–butadiene (CSBR) powdered rubber acted as a nucleating agent for PA6 crystallization in PA6/CSBR TPVs. The effect of dicumyl peroxide and MA on the crystalline beta-phase of isotatic PP/EPDM system was studied by Tang *et al.*[11] and the related results showed that the beta-phase content of iPP decreased sharply with the increase of MA content. However, the effect of how the processing additives affect the morphological aspects of semicrystalline TPV blends is still not completely understood.

Thermoplastics like PA6 have high modulus, good mechanical strength, dimensional stability at elevated temperature and chemical resistance to many moderately polar and nonpolar organic species. Used for special purposes, NBR has both good oil and abrasion resistance.[4,12] Blend combinations of these two components would be expected to have excellent hot oil resistance and good strength properties, particularly at elevated temperatures.[13,14] Thus, the effect of processing parameters and blend composition should be taken into account to evaluate the final properties in dynamically vulcanizated PA6/NBR blends.

Our research group has investigated dynamically vulcanizated PA6/NBR blends prepared by masterbatch mixtures, i.e., some additives were individually added to PA6 and NBR and the obtained masterbatches were blended. Some previous results indicated that processing additives, such as nonylphenol and EVA copolymer, reduce the total processing energy and contribute to achieve a well-defined morphology.[15] EVA is well-known additive in polymer blends, acting as auxiliary process additive as well as a compatibilizer.[16,17] However, on the basis of the published literature, there are few works devoted to investigate the effects of the processing additives on the crystallization behavior of PA6/NBR masterbatched blends. The aim of this work was to investigate the effect of different EVA-based additives in the PA6 masterbatch on the crystallization behavior and the microstructure of the thermoplastic matrix.

EXPERIMENTAL

NBR (acrylonitrile content of 28 mol %) was kindly supplied by Petroflex Ind. Com. S.A., now Lanxess, Brazil. PA6 (Radilon Natural S, MFI = 19.6 g/10 min) was kindly supplied by Radici Group, Brazil. Two different EVA copolymers, having vinyl acetate content of 18 mol % (EVA18) and 33 mol % (EVA33), were supplied by Brasken S.A., Brazil. EVA 28 mol % grafted with MA (EVAMA 0.8 mol %) was kindly supplied by Proquimil, Brazil. Phenolic resin (octylphenol–formaldehyde SP1045, Schenectady do Brasil, Itatiba, Brazil), stannous chloride, and Naugard 449 antioxidant (kindly supplied by Crompton Corporation do Brasil, Rio Claro, Brazil) were used to compose the NBR vulcanization system.

Prior to all melt processing steps, PA6 was dried under vacuum at 80 °C until it showed constant weight. Masterbatches were prepared at 80 rpm in the internal mixing chamber of a Brabender Plasticorder Rheometer (Germany) at 240 °C for PA6 masterbatches (MPA) and 40 °C for NBR masterbatches (MNBR). PA6 was melted first for 2 min before the addition of the different types of additives used in this study, which were used according to the formulations given in Table I. The mixing was then continued until a constant torque was obtained. In the case of MNBR, 10 phr of Naugard 449 antioxidant was directly mixed with NBR until constant torque.

Table I. Masterbatches Composition of PA6

		Additive	
Sample	PA6 (phr)	Type	Content (phr)
MPA	100	Naugard 449	10.0
MPA18	100	EVA18	5.0
MPA33	100	EVA33	5.0
MPAMA	100	EVAMA	5.0

Blends of PA6/NBR masterbatches were prepared at 220 °C in the internal mixing chamber of a Brabender Plasticorder Rheometer (Germany), using a blend ratio of masterbatches fixed at 50:50. The different MPA materbatches were melted first for 2 min before the addition of MNBR. After 2 min, NBR vulcanization system was added and the mixing was continued until a constant torque was obtained. The final composition of the PA6/NBR TPVs is summarized in Table II. The samples obtained were grounded in a Seibt cutting mill and molded in a Battenfeld Plus 35 injection machine under the following conditions: mold pressure, 110 bar; temperature of injection, 240 °C; injection pressure, 80 bar; back pressure, 50 bar. Prior to injection molding, all samples were dried under vacuum for 24 h at 100 °C.

Differential scanning calorimetry (DSC) experiments were performed using a Perkin–Elmer differential scanning calorimeter DSC 7 (Norwalk, CT., USA). Prior to analysis all samples were dried under vacuum at 80 °C overnight. Non-isothermal analyses were realized using a scan-mode method. The samples were heated at 20 °C/min from 40 to 260 °C, held isothermally for 5 min and then cooled at 20 °C/min to 40 °C. After 1 min, the samples were heated again using the same protocol of the first scan. Isothermal crystallization analyses of the PA6/NBR samples were performed. Samples were heated from 40 to 260 °C at 20 °C/min, held isothermally for 5 min to complete melting, then rapidly cooled to 200 °C, where the samples were allowed to crystallize for 15 min.

Wide angle X-ray scattering (WAXS) was performed using a Rigaku Miniflex diffractomer (Japan) with an incident X-ray

Table II. Final Composition of PA6/NBR 50:50 TPVs Samples

Sample	PA6 phase	NBR phase
M1	MPA	MNBR + vulcanization system (phenolic resin 5.0 phr + $SnCl_2$ 0.25 phr + Naugard 449 5.0 phr)
M4	MPA18	
M5	MPA33	
M6	MPAMA	

wavelength of 1.5418 Å at a scan rate of 0.05°/s. X-ray analyses were performed at room temperature. PeakFit software was used to deconvolute the obtained curves using a Lorentzian algorithm.

The infrared spectra of the samples were recorded by Varian Excalibur 3100 Fourier transform infrared (FTIR)-attenuated total reflection. Samples were placed in direct contact with the zinc selenite crystal. Spectra were collected with 2 cm^{-1} spectral resolution and twenty scans were performed for each sample. Viscoelastic properties of the blends were analyzed with a dynamic mechanical thermal analyzer (DMTA) Q800 TA Instruments (USA) operated in single cantilever mode within the temperature range of −50 to 80 °C (heating rate of 3 °C/min, constant frequency of 1 Hz, and 0.025% strain amplitude). The applied amplitude was considered in order to perform all measures within the linear viscoelastic region. Storage modulus (E'), loss modulus (E''), and damping coefficient (tan δ) data were collected as a function of temperature for all samples. All measures represent the average of two scans.

Positron annihilation lifetime spectroscopy (PALS) facility located at Federal University of Minas Gerais (Belo Horizonte, Brazil) was employed to characterize the free volume parameters of the matrix. The positron lifetime spectra were obtained using a conventional Ortec "fast–fast" coincidence circuit with 280 ps of time resolution, from the ^{60}Co prompt curve. ^{22}NaCl, of approximately 4 × 10^5 Bq activity, sandwiched between two 70.0 μm-thick foils of Kapton, was used as the positron source. Two samples of PA6/NBR in the form of sheets with ∼8 × 8 mm^2 area and 1.5 mm thickness were sandwiched between the positron source and the measurements were carried out at 21.0 °C. The lifetime spectra were satisfactorily resolved into three components using the POSITRON FIT EXTENDED program,[18] leading to the intensities (I_i) and lifetimes (τ_i) of the various positron states: subscripts 1, 2, and 3 refer to *para*-positronium (*p*-Ps), free positron, and *ortho*-positronium (*o*-Ps), respectively. The *o*-Ps lifetimes (τ_3) and intensities (I_3) were determined from the spectral analysis with all τ_1 fixed at 120 ps. The samples were measured in triplicate, with the mean value taken for each experiment. The lifetimes, obtained in the experimental spectrum analysis, are average values of the positronic species lifetimes distribution. All samples were analyzed in triplicate.

RESULTS AND DISCUSSION

The melting behavior of the PA6/NBR blends is shown in Figure 1 and Table III summarizes the obtained crystalline parameters. The degree of crystallinty of the samples was obtained by eq. (1):

$$X_c = \frac{\Delta H_m}{\Delta H_m^0 \cdot \phi} \quad (1)$$

where ΔH_m is the heat required for melting the sample, $\Delta H_m^0 = 230$ J/g[19] is the 100% crystalline heat of fusion of PA6 and ϕ is the volume fraction of PA6.

Non-isothermal DSC curves of the blends (second heating) showed two well separated melting peaks when compared to the pure PA6. Pure PA6 was processed under the same processing conditions as the MPA masterbatch as control. Several authors

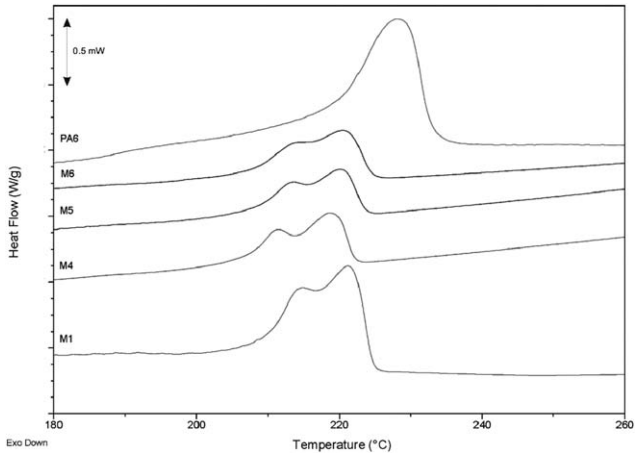

Figure 1. Heating scans of PA6 and PA6/NBR TPVs.

have considered the lower melting process observed in DSC as being related to the γ-crystalline form of PA6. Zhang and coworkers[10] have described the presence of γ-forms in PA6/ultrafine full-vulcanized rubber particles and similarly, Fornes and Paul[20] have observed the same feature in PA6/organically modified montmorillonite nanocomposites.

These two melting peaks suggest changes in crystalline thickness and its distribution, resulting in two individual populations of γ- and α-crystalline forms. The presence of the NBR vulcanized particles significantly affects the crystalline order of PA6. It is expected that the elastomer particles contribute to decrease of the intermolecular interaction of PA6 chains, resulting in a less ordered matrix. Moreover, incorporation of EVA18 and EVA33 additives did not contribute to extend the crystalline disorder of PA6 matrix, as can be seen in Table III. Nevertheless, it is interesting to note that the value for ΔH_m was slightly higher for M6 than the others EVA-based blends. Roeder *et al.*[21] have described the formation of imide linkage at the interface between PP-*g*-MA and PA6 in blends of PP/PP-*g*-MA/PA6. Similar interaction was observed by Bhattacharyya *et al.*[8] in blends of PA6 and EVAMA. Figure 2 shows the FTIR spectra of PA6, EVAMA, and M6 samples. The presence of the typical bands of EVA (1734 cm^{-1}, υC═O; 1237 and 1020 cm^{-1}, υC─O; 718 cm^{-1}, γCH) were confirmed. The characteristic band assigned to the symmetrical C═O stretching of anhydride unit was overlapped by the carbonyl carbon of the EVA. It is possible

Table III. Crystallization Parameters Obtained from DSC Analyses[a]

	T_m (°C)			
Sample	First peak	Second peak	ΔH_m (J/g)	X_c (%)
PA6	—	228.07	93.62	40.7
M1	215.16	221.25	29.30	25.8
M4	211.52	218.57	29.32	28.1
M5	213.80	220.03	26.96	25.1
M6	214.71	220.40	32.74	32.7

[a] The experimental errors associated with the thermal analysis experiments are ± 0.5 °C, ±0.81 J/g and 1.2% for T_m, ΔH_m, and X_c, respectively.

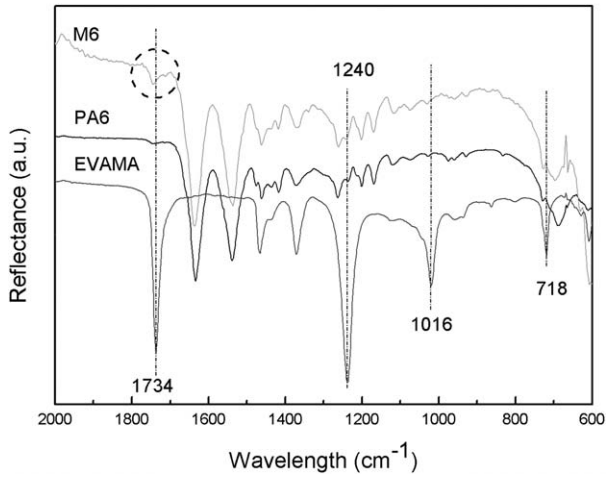

Figure 2. FTIR spectra of PA6, EVAMA, and M6 samples.

to observe that the bands associated to C—O stretching of EVA disappeared in M6 sample. However, the presence of a small band slightly shifted to 1745 cm^{-1} is an evidence of the imide linkage formed between PA6 and EVAMA. Thus, it seems that the grafting reaction of the MA groups in EVAMA onto the PA6 matrix contributes to diminish the disordered state achieved by the presence of NBR particles.

In order to further understand the crystallization behavior of the PA6 matrix, isothermal crystallization-time dependence was analyzed by the Avrami equation[22]

$$X_c(t) = 1 - \exp\left[-K(T)t^n\right] \quad (2)$$

where $K(T)$ is a kinetic constant and n is the Avrami exponential.

The effect of the presence of additives on crystallization kinetics can be evaluated by the time of half-crystallization, $t_{1/2}$ (Figure 3). For all samples (Table IV), the presence of EVA-based additives retarded the crystallization. This feature was expected, since specific interactions can diminish the amount of surface area available on which PA6 crystals are able to nucleate and grow. Table IV summarizes the crystallization parameters obtained from Avrami equation. It can be seen that the Avrami exponent n were slightly similar for the non-additive and additive samples with EVA18

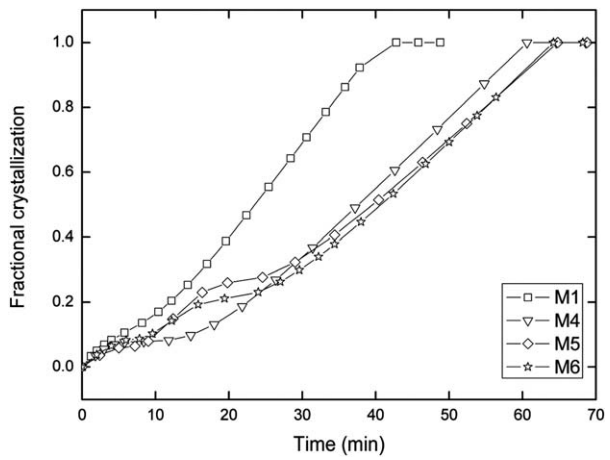

Figure 3. Fractional crystallization curves for non-additive (M1) and additive samples (M4–M6).

Table IV. Avrami Parameters Obtained from Isothermal DSC Analyses

	Avrami constants			
Sample	n	$K(T) \times 10^{-4}$ s^{-n}	$t_{1/2}$ (s)	ΔH_c (J/g)
M1	3.4	50.07	23.65	39.85
M4	3.5	48.15	38.35	51.05
M5	3.5	138.81	39.86	78.62
M6	4.5	14.46	40.95	75.67

and EVA33. However, the presence of MA significantly altered the crystal growth dimension of PA6 and the crystallization coefficient K also was smaller for the M6 sample. It seems that the formation of imide linkage contributed to maintain a higher cohesive level of the PA6 chains that allows more controlled crystal growth. The same effect was previously described by Biber *et al.*[23] in blends of nylon 6 and polyethylene–buthyl acrylate–MA copolymer. It is important to note that the obtained Avrami exponent n suggest only qualitative aspects of the crystal nucleation-growth mechanism. In the case of PA6, several factors as heating–cooling rate, relaxation of the crystalline regions, and secondary crystallization under isothermal conditions may influence the obtained n values.[24] Values of $n > 4$ for PA6 are related to increasing rate of nucleation, which is no longer constant throughout crystallization process.[25] Therefore, the presence of the imide linkages contributed as the main factor to this behavior.

The γ-crystalline form of PA6 arises from hydrogen bonds between parallel polymeric chains, resulting in a less stable pseudo-hexagonal lattice.[20,26,27] This type of lattice is commonly reported for rapid cooling rate and low crystallization temperature processes.[28,29] In WAXS scans [Figure 4(a)], the main crystalline reflection in pure PA6 corresponds to the overlapped crystal planes of γ- and α-crystals. As observed in DSC analyses, it is evident that the presence of the NBR particles altered the crystallinity of PA6 matrix [Figure 4(b) and Table III], resulting in broadening of the main reflection. However, incorporation of EVA-based additives resulted in two distinct peaks in the WAXS curves [Figure 4(c–e)]. It seems that the presence of EVA additives contributes to increase in the molecular mobility of the PA6 matrix during the crystal growth. This behavior is in agreement with the plasticization effect of EVA previously related by others authors.[16,17] Thus, the overall degree of crystallinity of these samples was lower when compared to the M1 samples. Nevertheless, diffraction pattern of M6 sample are slightly different. As can be seen in Figure 4(e), the diffraction intensity associated to the γ-crystals is higher when compared to the α-crystals. This feature indicates that the imide linkage contributes directly to increase the γ-crystal content and, therefore, increase the degree of crystallization observed simultaneously by DSC and WAXS. In order to confirm this, Table V shows the apparent lateral crystal size obtained after deconvolution of WAXS curves using the Scherrer equation[30]

$$l = \frac{0.89\lambda}{\beta \cos\theta} \quad (3)$$

where λ is the X-ray wavelength (1.5418 Å), β is the full width at half maximum obtained from the WAXS peaks, and θ is the

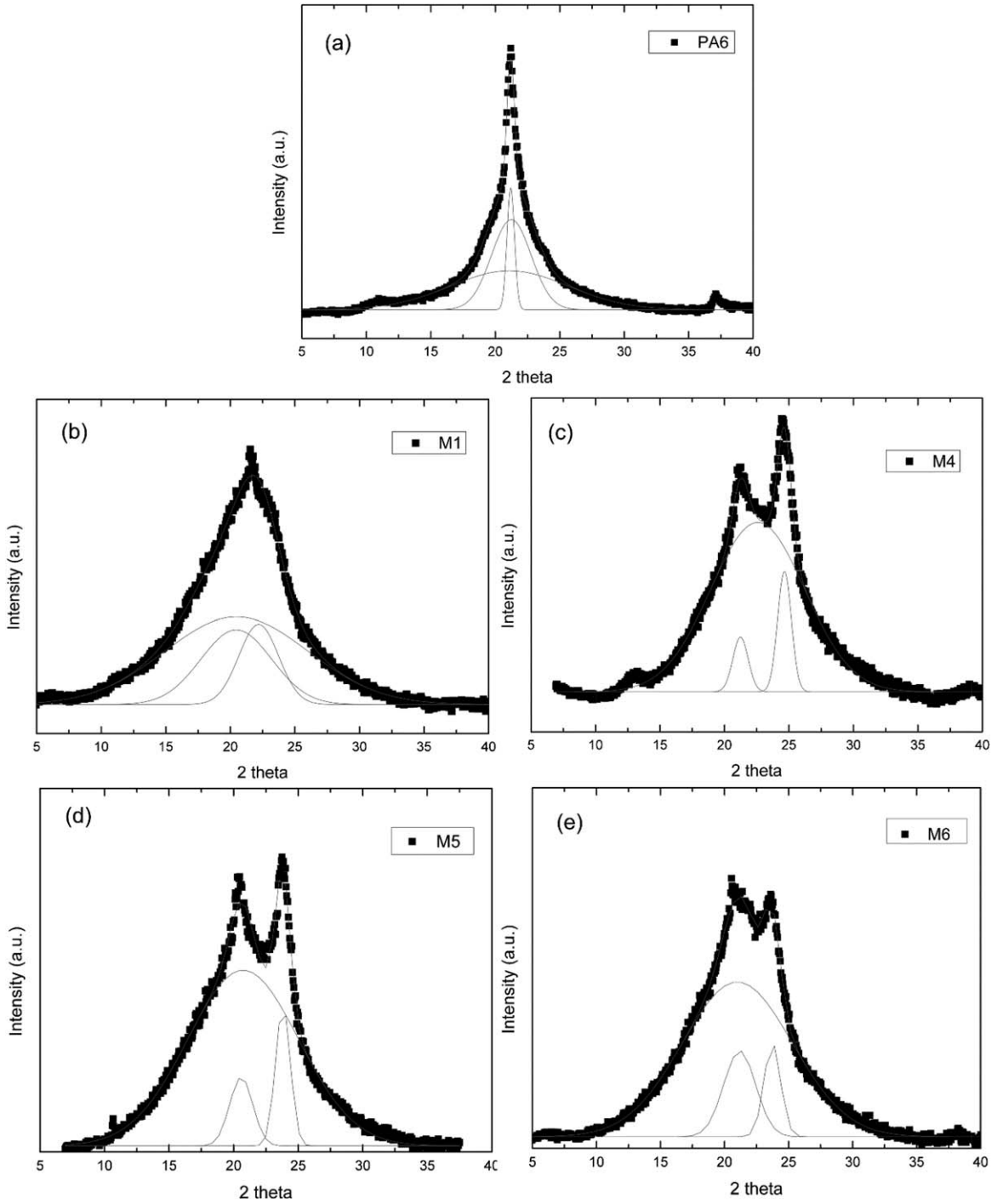

Figure 4. WAXS profiles and peak-fitting of PA6 and PA6/NBR TPVs.

diffraction angle. The overall degree of crystallinity of the samples was obtained as follows:

$$X_c(\%) = \left[\frac{A_c}{A_c + A_a}\right] \times 100 \quad (4)$$

where A_c and A_a are, respectively, the area under the crystal curve and the area under the amorphous curve. Deconvolution of the WAXS curves was obtained using a Lorentzian peak function. Peak-fitting of polymer with multiple crystalline forms, as polyamide and poly(ethylene terephthalate), should result in high level of uncertainty.[20,31] Since the use of initial guess for each peak calculation would be necessary, it is reasonable to treat the obtained values shown in Table V as approximated values.

NBR particles contributed to diminish the overall lateral crystal size. However, the incorporation of EVA additives resulted in

Table V. Crystal Parameters Obtained from WAXS Analyses

	X_c (±1.0%)			l (nm)	
Sample	Total	γ	α	γ	α
PA6	49.5	10.1	39.4	13.6	2.6
M1	40.3	25.1	15.2	1.4	2.6
M4	13.6	4.6	9.0	4.2	7.4
M5	15.8	6.8	9.0	4.4	7.0
M6	20.2	12.9	7.3	3.2	3.4

large crystals with similar dimensions. This behavior may be related to the plasticization effect, as discussed above. In the case of EVAMA additive, the formation of the imide linkage resulted in smaller lateral crystal size. This behavior is in agreement with a higher cohesive level in PA6 matrix. Same behavior was previously reported by Bhattacharyya *et al.*[8] in blends of PA6 and EVAMA. Therefore, the extension of the changes on the crystal parameters was more significant for EVAMA additives when compared to the others EVA-based additives in PA6/NBR blends.

PALS has been used for the characterization of systems at molecular level. Tao[32] and Eldrup *et al.*[33] showed a preferential localization of *o*-Ps into the free volume hole, based on the spherical potential wall and the *o*-Ps lifetime (τ_3) is directly related to the free volume radius (R). Assuming that the annihilation rate of the *o*-Ps inside the electron layer of width ΔR at the internal surface of the free volume is 2 ns^{-1}, we can use the following equation

$$\tau_3 = \frac{1}{2}\left[1 - \frac{R}{R_o} + \frac{1}{2\pi}\sin\left(2\pi\frac{R}{R_o}\right)\right]^{-1} \quad (5)$$

where $R_o = R + \Delta R$ is an empirical parameter equal to 1.66 Å.[34] Table VI shows the values of the positron annihilation parameters of TPVs samples, as calculated using eq. (5). As indicated by WAXS and DSC, the NBR particles contribute directly to diminish the ordered domains of PA6 matrix, resulting in higher amorphous fraction when compared to the pure PA6. In amorphous polymers, the *o*-Ps is preferentially formed and localized into the free volume holes, while in the crystalline phase *o*-Ps may be formed into interstitial free volumes at vacancy-type defects and on the crystalline–amorphous interfaces regions.[35–40] Therefore, increase in τ_3 values corresponds to higher segmental motion of the PA6 chains.[41,42]

Table VI. PALS Parameters Obtained for PA6/NBR Samples at 21 °C

Sample	τ_3 (ns)	I_3 (%)
PA6	1.55 ± 0.01	20.4 ± 0.2
M1	1.84 ± 0.02	16.0 ± 0.2
M4	1.91 ± 0.01	19.9 ± 0.1
M5	1.90 ± 0.02	18.9 ± 0.3
M6	1.88 ± 0.01	17.5 ± 0.3

Table VII. Analysis of DMA Curves of PA6 and PA6/NBR Blends

	T_g (°C)		Normalized ΔH_a[a]	
Sample	PA6	NBR	PA6	NBR
Pure PA6	16.8	—	—	—
Pure NBR	—	−15.7	—	—
M1	7.8	−12.8	2.3	0.4
M4	−5.6	−12.7	3.1	0.7
M5	−1.6	−13.2	3.1	0.5
M6	9.6	−17.6	5.4	0.5

[a] Values were normalized by the ΔH_a obtained for pure PA6 and NBR.

The role of EVA additives acting as plasticizers for the PA6 matrix was confirmed by PALS. For all EVA-based samples a significant increase of the free volume occurs. On the other hand, the values of τ_3 decrease slightly for M6 sample, indicating that the presence of imide linkage in EVAMA–PA6 interface reduces the available free volume of the matrix. PALS analyses confirmed the microstructure parameters previously observed by DSC and WAXS.

An interesting methodological approach to correlate the viscoelastic contribution of the blend components to the mechanical properties was proposed by Chang *et al.*[43] The area under the loss modulus (A_{los}) curve versus temperature in the glass transition region obtained by DMTA analyses may be directly related to the activation enthalpy of relaxation of the molecular motion in the amorphous phase (ΔH_a). The proposed model may be described by eq. (6)

$$A_{loss} = \frac{(\ln E''_G - \ln E''_R)\pi R T_g^2}{2(\Delta H_a)} \quad (6)$$

where E''_G and E''_R are the loss modulus in the glassy and rubbery state, respectively, R is the gas constant, and ΔH_a is the activation enthalpy of the glass transition process. Therefore, changes in the activation enthalpy of the PA6 matrix caused by the presence of both NBR particles and the EVA-based additives may indicate substantial changes in the blend microstructure. Table VII shows the values of T_g and the ΔH_a for the blends. When compared to the pure PA6 (16.8 °C) and pure NBR (–17.6 °C), the obtained values of T_g in M1 samples showed clearly the effect of the dynamic vulcanization in the NBR particles. Thus, the dynamic-mechanical behavior of M1 sample is in agreement with the WAXS, PALS, and DSC results. The plasticization effect of the EVA additives on the PA6 matrix was confirmed by the significantly diminishing in the PA6 phase T_g. However, the increasing value of PA6 phase T_g in M6 blend when compared to the other EVA additives confirms the presence of the imide linkage between MA groups of EVAMA and PA6. The values of ΔH_a were normalized in terms of the individual PA6 and NBR activation enthalpies. Hence, the normalized values may be quantitatively discussed. Normalized activation enthalpy showed that the presence of NBR vulcanized particles and EVA additives affect predominantly the molecular motions of the PA6 phase. Besides, the plasticization effect of EVA additives also

contributes to increase the mechanical damping of the blends M4 and M5 (higher values of ΔH_a). For the M6 sample, the higher ΔH_a reflects the presence of interfacial interactions that enhance the mechanical damping when compared to the others EVA additives. In the case of the NBR phase, small values of ΔH_a confirms the dynamic vulcanization of the elastomer, since the crosslinked chains show intrinsically low level of molecular mobility.

CONCLUSIONS

On the basis of our results, the addition of EVA-based additives and the dynamic vulcanization of the NBR contribute directly to the change in the crystallinity of PA6 matrix. Evidences of this crystalline disorder were provided by the presence of NBR vulcanized particles, resulting in less-ordered crystals. However, EVA additives play an important role in the molecular mobility since they act as plasticizers of PA6 matrix and decreased the overall degree of crystallinity of the TPV. On the other hand, EVA-*g*-MA shows an interesting behavior associated to the imide linkage formation at the additive/matrix interface. WAXS, DSC, PALS, and DMTA results show that changes in the molecular mobility of PA6 matrix in PA6-EVAMA/NBR TPV contribute to form less disordered γ-crystals with higher viscoelastic damping when compared to the other EVA-based additives. Regarding the analyses, it is very important to emphasize that the PALS technique proved to be an interesting and effective tool in monitoring free volume changes in PA6/NBR TPV systems.

ACKNOWLEDGMENTS

This work was supported by Conselho Nacional de Desenvolvimento Científico e Tecnológico (CNPq) and Fundação de Amparo à Pesquisa do Estado de Minas Gerais (FAPEMIG).

REFERENCES

1. Mehrabzadeh, M.; Buford, R. P. *J. Appl. Polym. Sci.* **1996**, *64*, 1605.
2. Mehrabzadeh, M.; Delfan, N. *J. Appl. Polym. Sci.* **2000**, *77*, 2057.
3. Gessler, A. M.; Haslett, W. H., Jr. (to Exxon Co.). U.S. Pat. 3,037,954A (**1962**).
4. Coran, A. Y.; Patel, R. *Rubber Chem. Technol.* **1980**, *53*, 781.
5. Utracki, L. A. Polymer Alloys and Blends: Thermodynamics and Rheology; Hanser Publishers: Munich, Germany, **1989**; p. 52.
6. Nelb, R. G.; Chen, A. T. In Thermoplastic Elastomers, 3rd ed.; Holden, G., Kricheldorf, H. R., Quirk, R. P., Eds.; Hanser Publishers: Munich, Germany, **2004**; Chapter 9, p. 229.
7. Joseph, A.; George, S.; Joseph, K.; Thomas, S. *J. Appl. Polym. Sci.* **2006**, *102*, 2067.
8. Bhattacharyya, A. R.; Ghosh, A. K.; Misra, A.; Eichhorn, K. J. *Polymer* **2005**, *46*, 1661.
9. Liu, X.; Huang, H.; Zhang, Y.; Zhang, Y. X. *Polym. Polym. Compos.* **2003**, *11*, 449.
10. Zhang, X.; Liu, Y.; Gao, J.; Huang, F.; Song, Z.; Wei, G.; Qiao, J. *Polymer* **2004**, *45*, 6959.
11. Tang, X. G.; Yang, W.; Shan, G. F.; Xie, B. H.; Yang, M. B.; Fu, Q. *J. Macromol. Sci. B* **2007**, *46*, 841.
12. George, J.; Neelakantan, N. R.; Varughese, K. T.; Thomas, S. *J. Appl. Polym. Sci.* **2006**, *100*, 2912.
13. Kumar, C. R.; Nair, S. V.; George, K. E.; Ommen, Z.; Thomas, S. *Polym. Eng. Sci.* **2003**, *43*, 1555.
14. Kumar, R.; George, K. E.; Thomas, S. *J. Appl. Polym. Sci.* **1996**, *61*, 2383.
15. Gomes, A. C. O.; Soares, B. G.; Oliveira, M. G.; Oliveira, M. F. L.; Paranhos, C. M. *e-Polymers* **2009**, *9*, 106.
16. Moreira, V. X.; Soares, B. G.; Gomes, A. C. O.; Oliveira, M. G. *Rubber Chem. Technol.* **2005**, *78*, 1.
17. Soares, B. G.; Almeida, M. S. M.; Guimarães, P. I. C. *Eur. Polym. J.* **2004**, *40*, 2185.
18. Kirkegaard, P.; Eldrup, M. *Comput. Phys. Commun.* **1981**, *23*, 307.
19. Penel-Pierron, L.; Depecker, C.; Séguéla, R.; Lefebvre, J. M. *J. Polym. Sci. Part B: Polym. Phys.* **2001**, *39*, 484.
20. Fornes, T. D.; Paul, D. R. *Polymer* **2003**, *44*, 3945.
21. Roeder, J.; Oliveira, R. V. B.; Gonçalves, M. C.; Soldi, V.; Pires, A. T. N. *Polym. Test.* **2002**, *21*, 815.
22. Avrami, M. *J. Chem. Phys.* **1941**, *9*, 177.
23. Biber, E.; Gündüz, G.; Mavis, B.; Colak, U. *Mater. Chem. Phys.* **2010**, *122*, 93.
24. Di Lorenzo, M. L.; Silvestre, C. *Prog. Polym. Sci.* **1999**, *24*, 917.
25. Balamurugan, G. P.; Maiti, S. N. *J. Appl. Polym. Sci.* **2008**, *107*, 2414.
26. Xiuyan, R.; Guangfeng, W.; Li, L.; Xiyan, Z. *J. Elastom. Plast.* **2011**, *44*, 79.
27. Varlot, K.; Reynaud, E.; Kloppfer, M. H.; Vigier, G.; Varlet, J. *J. Polym. Sci. Part B: Polym. Phys.* **2001**, *39*, 1360.
28. Murthy, N. S.; Aharoni, S. M.; Szollosi, A. B. *J. Polym. Sci. Part B: Polym. Phys.* **1985**, *23*, 2549.
29. Murthy, N. S. *Polym. Commun.* **1991**, *32*, 301.
30. Guinier, A.; Fournet, G. Small-Angle Scattering of X-Rays; Wiley: New York, **1955**; p. 594.
31. Raabe, D.; Chen, N.; Chen, L. *Polymer* **2004**, *45*, 8265.
32. Tao, S. J. *J. Chem. Phys.* **1972**, *56*, 5499.
33. Eldrup, M.; Lightbody, D.; Sherwood, J. N. *Chem. Phys.* **1981**, *63*, 51.
34. Nakanishi, H.; Wamg, S. J.; Jean, Y. C. In Positron Annihilation Studies of Fluids; Sharma, S. C., Ed.; World Scientific: Kuala Lumpur, Malaysia, **1989**; p. 292.
35. Dlubek, G.; Alam, M. A.; Stolp, M.; Radusch, H. J. *J. Polym. Sci. Part B: Polym. Phys.* **1999**, *37*, 1749.
36. Machado, J. C.; Silva, G. G.; Soares, L. S. *J. Polym. Sci. Part B: Polym. Phys.* **2000**, *38*, 1045.
37. Hristov, H. A.; Yee, A. F.; Gidley, D. W.; Kitano, Y. In Proceedings of the American Physical Society—Annual Meeting, Syracuse, USA, March **1996**.

38. Misheva, M.; Djourelov, N.; Dimitrova, A.; Zamfirova, G. *Macromol. Chem. Phys.* **2000**, *201*, 2348.

39. Dlubek, G.; Bondarenko, V.; Pionteck, J.; Kilburn, D.; Pompe, G.; Taesler, C.; Redmannb, F.; Pettersb, K.; Krause-Rehbergb, R.; Alamd, M. A. *Radiat. Phys. Chem.* **2003**, *68*, 369.

40. Porto, A. O.; Silva, G. G.; Magalhães, W. F. *J. Polym. Sci. Part B: Polym. Phys.* **1999**, *37*, 219.

41. Bartoš, J.; Šauša, O.; Schwartz, G. A.; Alegría, A.; Alberdi, J. M.; Arbe, A.; Krištiak, J.; Colmenero, J. *J. Chem. Phys.* **2011**, *134*, 164507.

42. Dębowska, M.; Pigłowski, J.; Ślusarczyk, C.; Rudzińska-Girulska, J.; Suzuki, T.; Yu, R. *Radiat. Phys. Chem.* **2007**, *76*, 325.

43. Chang, M. C. O.; Thomas, D. A.; Sperling, L. H. *J. Appl. Polym. Sci.* **1988**, *34*, 409.